Hindawi
Mathematical Problems in Engineering
Volume 2021, Article ID 8842898, 15 pages
https://doi.org/10.1155/2021/8842898

Research Article

Transient Fluid-Solid Interaction and Heat Transfer in a Cavity with Elastic Baffles Mounted on the Sidewalls

Ahmad Haghani,[1] **Mehdi Jahangiri**,[1] **Rouhollah Yadollahi Farsani**,[1] **Ayoub Khosravi Farsani**,[2] **and Jalal Fazilatmanesh**[1]

[1]*Department of Mechanical Engineering, Shahrekord Branch, Islamic Azad University, Shahrekord, Iran*
[2]*Department of Mechanical Engineering, Faculty of Boroujen, Technical and Vocational University (TVU), Shahrekord, Chaharmahal and Bakhtiari, Iran*

Correspondence should be addressed to Rouhollah Yadollahi Farsani; r.yadollahi@iaushk.ac.ir

Received 13 July 2021; Revised 5 November 2021; Accepted 12 November 2021; Published 27 December 2021

Academic Editor: Amer Rasheed

Fluid-solid interaction phenomenon study is necessary for the analysis of several engineering systems such as structures and vessels that interact with wind and blood flow, respectively. In this study, the interactions between buoyancy-driven airflow and elastic baffle(s) inside a square enclosure were modeled numerically. While the two sidewalls of the enclosure were insulated, the lower and upper walls were kept at hot and cold temperatures, respectively. The heat transfer rate through the hot wall by calculating the Nusselt number and von Mises stress at the baffles' root for various configurations of baffle(s) was considered. The domain was modeled in ANSYS Workbench, and the k-ε model was employed to solve the turbulent convective flow ($Ra > 10^7$). A two-way algorithm along with the finite element method was employed to simultaneously solve the equations governing the fluid flow and the solid phase. The dynamic mesh method was employed to account for the change in the location of the fluid domain at a new time step. The results show the elastic baffle, in comparison to solid baffle, intensifies the heat transfer rate by 15%. The results also indicate that the Nusselt number in the single-baffle case is higher than in double-baffle cases. The fact that the amount of von Mises is a function of the baffles' configuration is another point obtained from the results. It was found that the von Mises stress at the baffles' root represents more unsteady fluctuations in the asymmetric case, while it approaches a constant value in the symmetric case.

1. Introduction

Natural convection derived by buoyancy forces is considered a fundamental classic problem in heat transfer and fluid dynamics inside enclosures with unequal wall temperatures [1]. In fact, it is observed in industrial applications such as solar collectors and cooling systems mounted on electronic equipment [2]. The simplified model consisting of a two-dimensional square enclosure in a laminar flow has been practically analyzed from various aspects [3–5]. These studies along with many other early works considered the solution to this problem using the steady-state assumption [6–8]. However, the free convection flow inside an enclosure has got a transient nature, and hence, time-dependent analysis of this problem has attracted researchers' attention.

The fluid flow regime (laminar or turbulent) inside an enclosure breaks through a considerable effect on heat transfer through the enclosure [9]. As a result, the heat transfer rate can be increased or decreased by creating turbulence in the fluid flow. Therefore, mounting fins or baffles on the sidewalls have been extensively considered one of the simplest techniques for enhancing heat transfer inside enclosures.

A newer approach to study convection flow inside an enclosure, which has become a topic of more interest in recent years, is incorporating an elastic solid object and investigating fluid-solid interactions. Examples of such

researches are tabulated in Table 1 including recent works on analyzing the effects of rigid as well as elastic baffle(s) on the heat transfer inside an enclosure.

A review of recent studies shows that no previous research has considered the interaction effects of two elastic baffle(s) on natural convective heat transfer and the flow field inside an enclosure. Therefore, the main objective is to accurately analyze the heat transfer and fluid flow and two-way affection of elastic baffle(s) mounted on the walls using a numerical approach. Moreover, a comparison of rigid and elastic baffles, an analysis of dominant heat transfer mechanisms, a comparison between the single- and double-baffle cases, and an analysis of variations in the dimensions of baffle(s) and location are also carried out.

2. Problem Description

As shown in Figure 1, an enclosure with the dimension of A is insulated on its two sidewalls and is thermally connected from the top and bottom to a cold source at temperature T_c and a hot source at temperature T_h, respectively. A baffle of length L and uniform thickness 0.15 A is mounted on one or two sides of the enclosure.

The temperature gradient at the top and bottom sides causes the fluid inside the enclosure to move due to buoyancy forces. This fluid flow inside the enclosure creates a pressure gradient imposing a force on the elastic baffle(s) and causing it to deform and generate interior stress. The baffle deformation pushes the fluid, which creates a secondary flow. This interaction continues during heat transfer until the strain energy of the baffle(s) would be balanced out by the fluid-driven forces. Cavities with different boundary conditions simply can be observed in many applications such as cooling and heating industries. These configurations were mentioned by many researchers [19, 22, 23] but not with elastic baffles to investigate natural heat transfer.

The governing circumstance numerical investigation of this problem would be a real challenging task: while the free convection affects the displacement of the baffle, the baffle causes a displacement through the fluid in turn, which itself influences the movement of baffle(s), finally. This study analyzed this interaction at every time step. The aim was to develop a logical understanding of heat transfer in the presence of another source of fluid flow and its interaction with buoyancy flows.

To the authors' knowledge, the present study is the first research to simultaneously consider the von Mises stress and average Nusselt number in various configurations of baffle(s).

3. Governing Equations

With regard to the basic assumptions, this study numerically simulated the two-dimensional, turbulent, time-dependent, and transient flow of an incompressible Newtonian fluid. With the exception of air density, which was modeled using the Boussinesq assumption, all the other thermophysical properties were assumed time-independent. Being the same as displacement and energy equations for elastodynamic structures, the equations governing the solid phase (i.e., the baffle(s)) are written as follows [24–26]:

$$\rho_s \frac{\mathrm{d}^2 d_s}{\mathrm{d}t^2} - \nabla\sigma = F_v, \tag{1}$$

$$\frac{\partial T}{\partial t} = \alpha_s \nabla^2 T, \tag{2}$$

where σ represents the stress tensor, d_s is the solid displacement vector, and F_v is the resultant volumetric force on the solid object. Using the linear elastic assumption for the baffle(s) and taking into account the geometric non-linearities, one can write the stress tensor as follows [27–29]:

$$\sigma = J^{-1} F S F^T, \tag{3}$$

where

$$\begin{aligned} J &= \det(F), \\ F &= (I + \nabla d_s). \end{aligned} \tag{4}$$

Moreover, the second Piola–Kirchhoff stress tensor S is related to strain by

$$S = C{:}\ (\varepsilon), \quad \varepsilon = 0.5\left(\nabla d_s + \nabla d_s^T + \nabla d_s^T \nabla d_s\right), \tag{5}$$

where $C = C(E^*, \vartheta)$. In the present problem, F_v in (1) represents the gravitational forces per unit volume of the fluid. It can be rewritten as follows [30, 31]:

$$F_v = \rho_s \cdot g. \tag{6}$$

Basic equations governing the fluid flow are the conservation of mass and momentum equations and the energy equation. Given the assumptions described above, the physics of the flow is described by the following equations consisting of a set of partial differential equations with spatial and temporal variables. An Euler–Lagrangian representation can summarize these equations as follows [32–35]:

$$\nabla u = 0, \tag{7}$$

$$\frac{\partial u}{\partial t} + u.\nabla u = \frac{-1}{\rho_f}\nabla P + \vartheta_f \nabla^2 u + \beta g (T - T_c), \tag{8}$$

$$\frac{\partial T}{\partial t} + u.\nabla T = \alpha_f \nabla^2 T, \tag{9}$$

where u is the fluid velocity vector, P is the fluid pressure, and T represents the temperature of the solid or fluid. Moreover, ρ_s and ρ_f represent the solid and fluid densities, respectively, whereas α_s and α_f are the thermal diffusions of the solid and fluid, respectively. Kinematic viscosity and gravitational acceleration are denoted by ϑ_f and g_y, respectively, and β represents the coefficient of volumetric expansion. It should be noted that (9) assumes a Newtonian fluid and a linear relationship between shear stress and strain rate.

The equation for transfer of turbulent kinetic energy in the software is given by [36–39]:

$$\frac{\partial \rho\, k}{\partial t} + \frac{\partial \rho\, u_j k}{\partial x_j} = \frac{\partial}{\partial x_j}\left(\mu \frac{\partial k}{\partial x_j}\right) + \frac{\partial}{\partial x_j}\left(\frac{\mu_t}{\sigma_k}\frac{\partial k}{\partial x_j}\right) + \mu_t\left(\frac{\partial \overline{u}_i}{\partial x_j} + \frac{\partial \overline{u}_j}{\partial x_i}\right)\frac{\partial \overline{u}_i}{\partial x_j} - \rho\varepsilon. \tag{10}$$

Furthermore, the transfer equation for eddy dissipation rate is expressed as follows [40]:

$$\frac{\partial \rho\, \varepsilon}{\partial t} + \frac{\partial \rho\, C_j \varepsilon}{\partial x_j} = \frac{\partial}{\partial x_j}\left(\left(\mu + \frac{\mu_t}{\sigma_\varepsilon}\right)\frac{\partial \varepsilon}{\partial x_j}\right) + \frac{\varepsilon}{k}\left(C_{\varepsilon 1}\tau_{ij}\frac{\partial C_i}{\partial x_j} - C_{\varepsilon 2\rho\varepsilon}\right) \tag{11}$$

which contains a number of empirical coefficients determined through some basic experiments, including boundary layer experiments over a flat surface. The values of these coefficients are as follows [40]:

$$\begin{aligned} C_\mu &= 0.09, \\ \sigma_k &= 1.0, \\ \sigma_\varepsilon &= 1.30, \\ C_{1\varepsilon} &= 1.44, \\ C_{2\varepsilon} &= 1.92. \end{aligned} \tag{12}$$

When multiple iterations of the coupling are made within one coupling step, full convergence in the fluid domain is necessary for every iteration, until the final iteration of the coupling converges. The flowchart in Figure 2 illustrates this reciprocating process better.

4. Simulation Requirements

The necessary steps were taken using the Workbench section of ANSYS software to analyze the problem of fluid-solid interaction in a two-dimensional rectangular enclosure under free convection induced by a temperature difference between the enclosure's walls.

A comparison was carried out to validate the simulation and assurance before deriving the results. Therefore, the configuration shown in Figure 3 according to the study of [41] was chosen, and the results including the streamlines were given in Re number of 1,000. As it can be observed, a good agreement exists between the present simulation and the mentioned study.

The analysis results of the case with a single elastic baffle are presented in Figure 4 for grids having 7,657, 12,405, and 15,350 elements. The different numbers of elements were selected based on different mesh sizes. In the present work according to the geometry of the problem, only in the areas close to the elastic baffles that are sensitive areas, the number of the computational grid is important, and therefore, only in these areas, the grid has become finer by a factor of 2.

The variation trend of the von Mises stress for these three girds shows that the one with 12,405 elements can be selected to be used in further calculations. Figure 5 shows the type of elements considered. The internal domain was discretized using triangular elements, and refined elements were used in the boundary layers and around the baffles. Furthermore, the baffles were meshed using tetrahedron elements. A general view of the solution domain and the mesh style is shown in Figure 5.

For the system with the properties of Intel(R) Core(TM) i5-1035G1 CPU: 1.19 GHz, RAM: 8.00 GB (7.81 GB usable), the time step of 0.01, and the 12,405 grids; each time step consumes 13 s to converge.

It should be noted that solid analyses are far less grid-dependent than fluid analyses. However, the same steps were taken to select the suitable mesh size within the baffles, which ultimately resulted in 650 structured elements on the solid baffles.

By calculating variations of the von Mises stress as a major variable over time for different time steps values (i.e., 0.1, 0.05, 0.01, and 0.005 s), it was concluded that a time step of 0.005 s can predict the results more accurately in optimum time.

Fluid domain equations along with their associated boundary conditions were discretized using the control volume method. Second-order and implicit first-order discretization techniques were used for space and time discretization, respectively, in the momentum and energy equations. Moreover, the equations were simultaneously solved using the two-way coupled algorithm. At each time step, fluid domain equations were solved to determine the forces imposing on the baffle. With these forces and other associated boundary conditions available, baffle motion equations were solved using the finite element method and the Newton–Raphson iterative technique to determine the displacement of each point on the baffle. Since these displacements cause deformation in the fluid domain, a new computational mesh was generated through the "dynamic mesh method" in the next time step. In order to accurately follow the fluid-solid interface at various time steps, an unstructured triangular grid along with boundary layer elements was used near the walls.

The baffle(s) are assumed to be formed of rubber with the modulus of elasticity of 4 MPa that is guaranteed to be loaded limited to an elastic range. The hot and cold wall temperatures were considered 440 and 300 K, respectively. The Rayleigh number of $\mathrm{Ra} = 1.75 \times 10^7$ was calculated based on the temperature difference and air properties. Therefore, the flow inside the enclosure was assumed to be turbulent and was modeled using the k-ε. Other assumptions of the numerical solution algorithm are summarized in Table 2.

The boundary condition for the fluid-solid interface on the baffle(s) surface, which results from the conservation of kinematic forces and dynamic displacements, is combined with the non-slip condition on the baffle(s) surface to yield as follows:

Table 1: Recent studies on the analysis of the effects of rigid and elastic baffles on heat transfer inside an enclosure.

Baffle type	Authors [ref.] (year)	Convection type	Fluid	Solution method	Problem statement	Main result
Solid	Asl et al. [10]	Natural	Air	Finite volume code	Effect of porous and solid fins in a rectangular enclosure	Porous and solid fins increase average Nusselt up to 41% and 20%, respectively.
Solid	Bendaraa et al. [11]	Natural	Copper-water nanofluid	COMSOL software	Effect of different locations of fins on heat transfer in a square cavity	Adding fins on the adiabatic/cold and hot walls increases and decreases average Nusselt, respectively.
Solid	Menni et al. [12]	Force	Air	Fluent software	Effect of baffle orientation and geometry on the heat transfer in a rectangular channel	The largest variation in Nusselt and skin friction has occurred in the region facing the baffle.
Solid	Keramat et al. [13]	Natural	Air	ANSYS fluent software	Effect of porous fins in H-shape cavity	Average Nusselt for porous fins increases by 60% in comparison to solid fins.
Solid	Li et al. [14]	Natural	Al_2O_3-water nanofluid	Fortran code	Effect of magnetic field and thermal radiation on the nanofluid around a circular baffle in a square cavity	Increasing the Hartmann and Rayleigh reduced heat transfer and improved Nusselt, respectively.
Solid	Gokulavani et al. [15]	Natural	Air	Finite difference code	Effect of the heated baffle on the fluid in the ventilation cavity	Vertical baffle transfers heat better than horizontal baffle.
Elastic	Ghalambaz et al. [16]	Natural	Air	Finite element code	Effect of horizontal oscillating baffle(s) on the heat transfer in a square cavity	Increasing the amplitude of oscillating baffle(s) significantly enhances Nusselt.
Elastic	Alsabery et al. [17]	Natural	Air	Finite element code	Effect of oscillating baffle(s) mounted on the bottom of the oblique cavity	Baffle(s) has (have) an essential effect on the flow and heat transfer.
Elastic	Raisi and Arvin [18]	Natural	Air	Numerical code	Effect of adiabatic and flexible baffle in the center of the cavity	An increase in Rayleigh increases the elastic baffle deformation.
Elastic	Hussein et al. [19]	Natural	Al_2O_3-water and Cu-water nanofluid	Fortran code	Effect of baffle length that horizontally attached to the left wall on the heat transfer	Baffle length changes flow field and vortices strength. The longer baffle causes more changes to the flow field.
Elastic	Ghalambaz et al. [20]	Natural	Newtonian fluid	Numerical code	Controlling the natural convection in the L-shape enclosure by flexible baffle	Stiffer baffle inhibits natural convection.
Elastic	Saleh et al. [21]	Natural	Porous medium and incompressible non-Newtonian fluid	Finite element code	Effect of the flexible baffle on the cavity filled with fluid and porous medium	With the rising oscillation amplitude, the heat transfer rate increases exponentially.

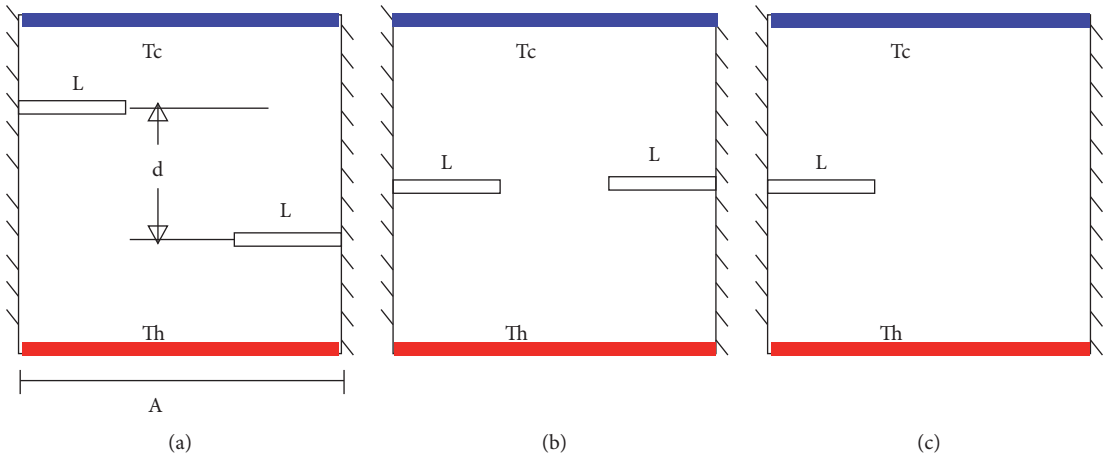

Figure 1: Problem geometries.

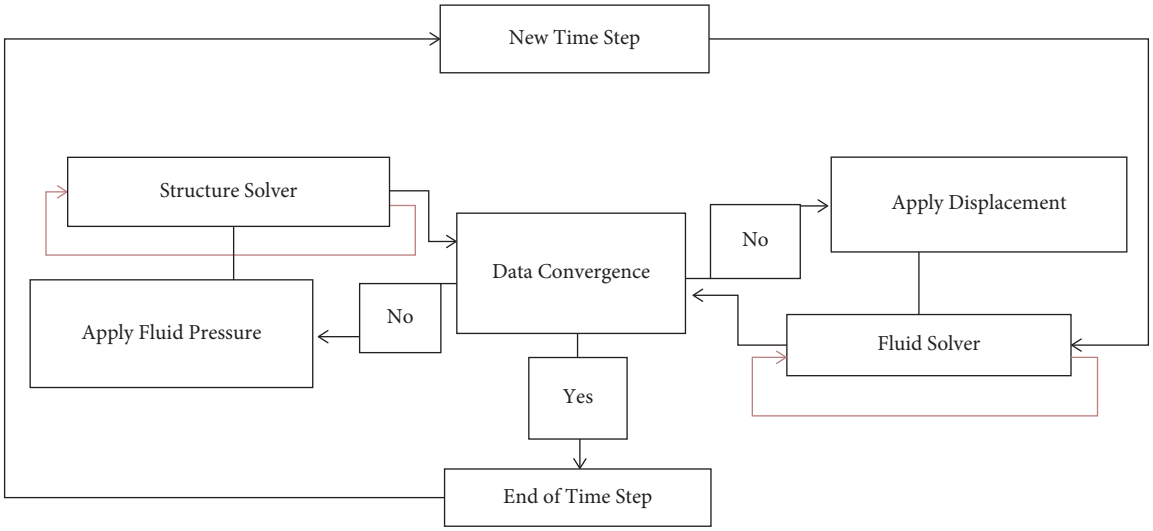

Figure 2: Two-way algorithm flowchart for the analysis of fluid-solid interaction.

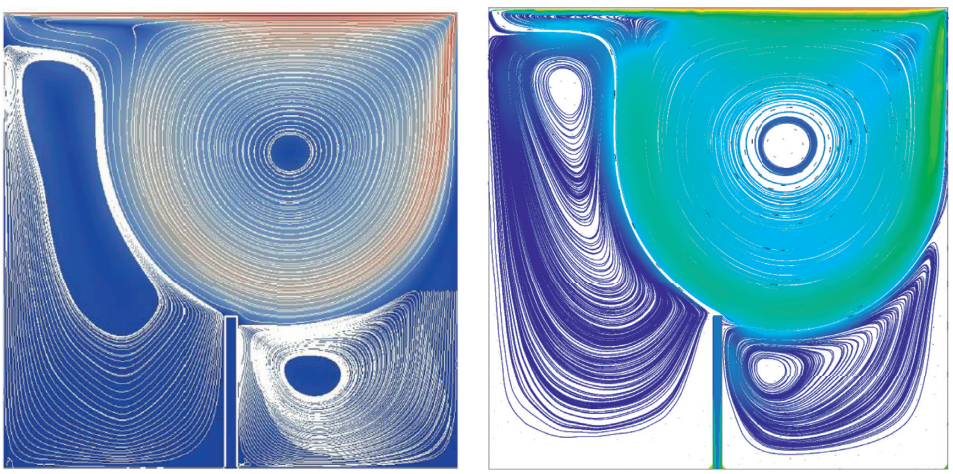

Figure 3: Single-component fluid flow in the cavity with an elastic (a) and present simulation (b) [41].

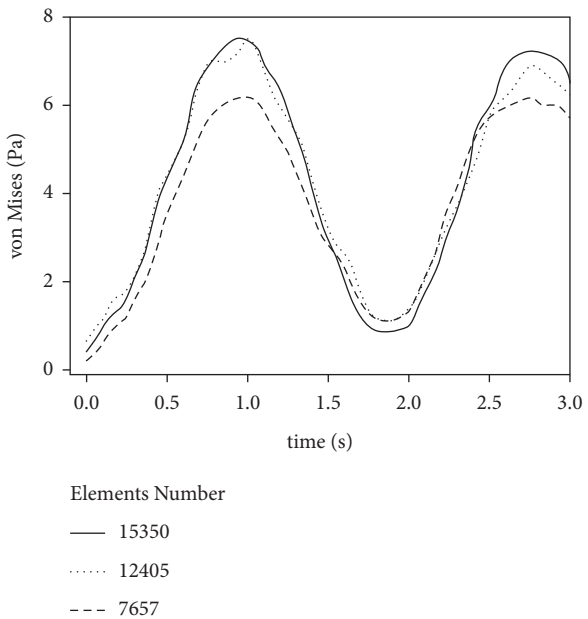

Figure 4: Effects of the number of elements on the von Mises stress for the single-baffle case.

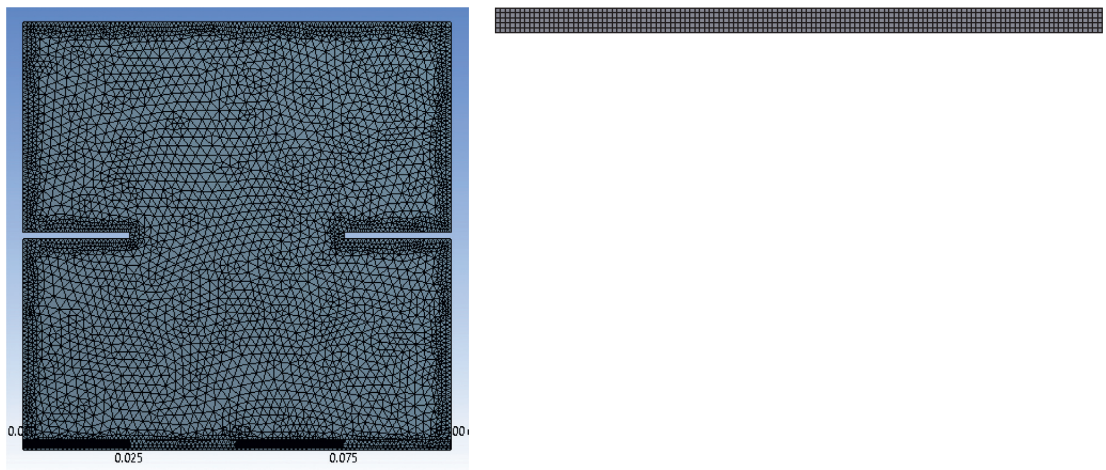

(a) (b)

Figure 5: Sample of meshed domain: (a) fluid domain and (b) elastic baffles.

Table 2: Features and techniques in the numerical solution algorithm.

Feature	Technique
Method of coupling velocity and pressure terms	Coupled
Temperature discretization	Second order
Pressure discretization	Standard
Momentum discretization	Second-order upwind
Energy discretization	Second-order upwind
Discretization of turbulence parameters (k, ε)	First-order upwind
Maximum number of iterations in the coupling	10
Mesh movement algorithm	Smoothing and remeshing
Mesh movement algorithm over the fluid-solid interface	System coupling and deforming

$$\frac{\partial d_s}{\partial t} = u, \qquad \sigma \cdot n = -P + \mu_f \nabla u. \tag{13}$$

The boundary condition for the clamped end of the baffle(s) is given by

$$\frac{\partial d_s}{\partial t} = 0. \tag{14}$$

Furthermore, assuming the fluid to be initially stationary yields the following initial condition:

$$u = 0. \tag{15}$$

The fluid phase specifications and solid properties used in this study are given in Tables 3 and 4.

5. Results

One of the applications would be in the cooling process of electronic components. So it was tried to distinguish the effect of elastic baffle(s) on the heat transfer from the bottom of the cavity. This study represents the two-way interaction of the heat transfer-driven flow and the oscillation of elastic baffle.

The average Nusselt number over the hot wall was selected to measure the quality of the convective heat transfer performance. First, the rigid and elastic baffles were investigated. Reference dimensions were considered $A = 0.1\,m$ and $L/A = 0.5$. The results at different time steps are shown in Figure 6. Since there is no change in the value of the Nusselt number after the time of 4 s, the time is limited to 6 s.

This analysis indicates that at an early time when the temperature difference is high, the Nusselt value takes a large value. This value decreases steadily during the time elapses. Moreover, the Nusselt number follows a higher value for the elastic baffle compared to the rigid baffle. This effect is a result of the fluid motion due to baffle fluctuations.

The results also show that the Nusselt number reaches a constant value that indicates a steady-state condition after the time of 2 s.

In the following, the effects of mounting baffles inside the enclosure are analyzed. Geometrical dimensions of the two baffles, including thickness and length, were similar to those in the single-baffle case, and the distance between the two baffles was equal to the distance of one baffle from the front side. Two cases of symmetric and asymmetric were considered for the vertical position of the baffles.

Figure 7 shows the steady-state flow pattern. Transferring heat from the bottom of the enclosure to the top in the single-baffle case, two vortices are observed in the upper and

Table 3: Thermophysical properties of the fluid used in the simulation.

Density (kg/m^3)	Coefficient of thermal expansion (1/K)	Kinematic viscosity (kg/m.s)	Conduction heat transfer coefficient (W/m.K)<
1.225	0.0032	2.6 e-5	0.0033

Table 4: Thermophysical properties of the solid used in the simulation [42].

Density (kg/m^3)	Young modulus (MPa)	Poisson's ratio	Conduction heat transfer coefficient (W/m.k)
1,200	4	0.45	60.5

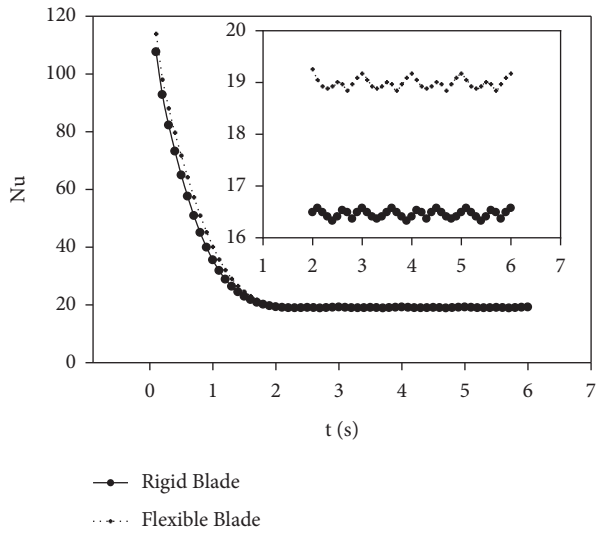

Figure 6: Comparison of the average Nusselt number over the hot wall for the cases with rigid and elastic baffles.

lower halves of the enclosure. In the symmetric double-baffles case, four vortices were developed at the top and bottom and on the left and right of the enclosure, whereas in the asymmetric double-baffle case, two small vortices were generated at the top and bottom, and a large vortex was generated between the cold and hot walls around the enclosure.

Time variations of the average Nusselt number over the hot wall are shown in Figure 8 for the three cases. The results indicate that the single-baffle and asymmetric double-baffle cases take the highest to lowest Nusselt numbers, respectively. According to Figure 8, baffle oscillations reach steady state after 15 s. Moreover, according to Figure 6, the Nusselt number remains in steady state after 4 s. Therefore, the authors believe that it does not need to continue the solution after 15 s, and the solution convergence is related to the simple geometry of the domain.

In the double-baffle cases, two vortices developed over the hot wall (Figure 7), which transfer less heat compared with the single-baffle case with a large vortex over the entire lower wall. We know that the larger the vortex between the hot and cold walls, the more the heat transfers, and the Nusselt number happens.

In the asymmetric case, the right baffle located closer to the hot wall causes a small vortex development at the bottom right corner, which restricts the large vortex laid between the upper and lower walls.

It must be noted that in the asymmetric case, the fluctuations in the Nusselt number are caused by fluctuating in the vortices' features and size. Figures 9–11 show the free convection flow pattern and velocity contours inside the enclosure for the three cases. Nevertheless, no significant variation is observed in the flow pattern for the single-baffle and symmetric double-baffle cases, the flow pattern for the asymmetric case experiences various fluctuations and changes, which results in small fluctuations in the Nusselt number.

The flow velocity is slightly more in the asymmetric case compared with the other two cases, which is due to the formation of small vortices on the upper and lower walls.

Figure 12 shows the von Mises stress in the baffle(s) versus time for the cases. Overall, the single-baffle case represents the highest average von Mises stress. This is due to the high convective heat transfer rate and hence is due to high compressive forces from the fluid on the baffle.

As the heat transfer mechanism became more stable over time (as reflected by the Nusselt number behavior), the von Mises stress was expected to also approach a constant value. However, further analysis indicated that the von Mises stress encounters some variations.

It is observed from the single-baffle case that the fluctuation amplitude experienced a gradually increasing trend after 8 s due to the hardening effect in the baffle and fluctuating transient loads from the vortices. In other words,

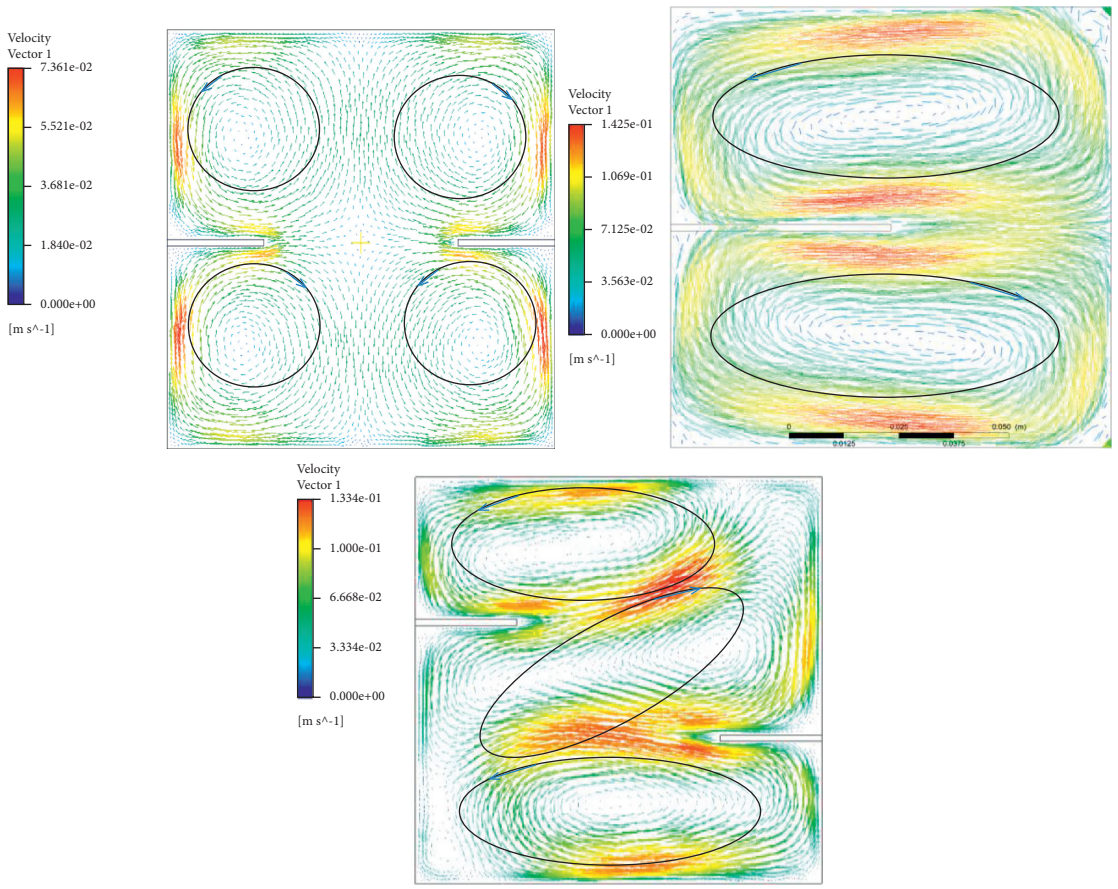

Figure 7: Streamline with the magnitude of velocity inside the enclosure for three cases: single-baffle, symmetric double-baffle, and asymmetric double-baffle (time = 6 s).

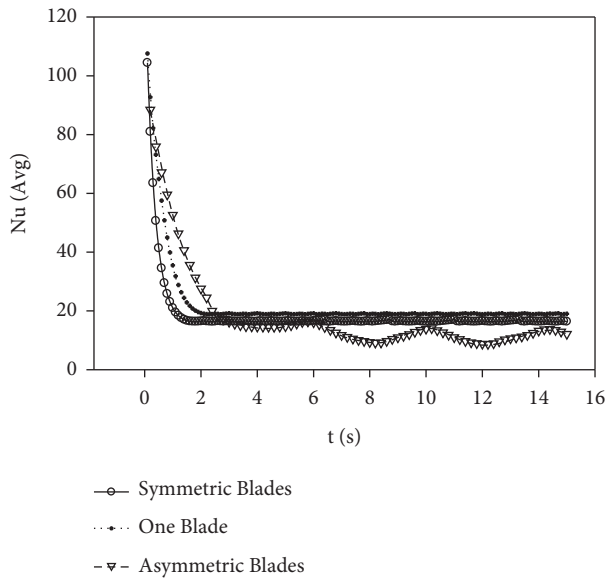

Figure 8: Time variations of the average Nusselt number over the hot wall.

variations in the size and features of vortices impose some unstable fluctuating forces on the baffles, which would ultimately lead to high cycle fatigue of the baffle. It is noted that the stress amplitude never reaches the yield stress limit of the baffle, and therefore, the baffle will not experience fatigue failure.

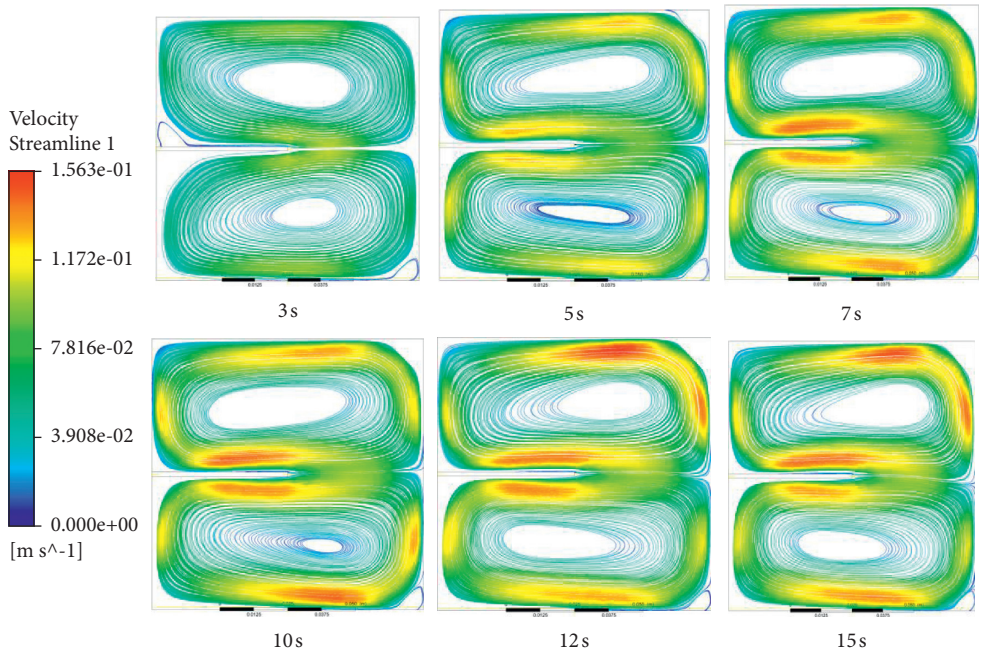

Figure 9: Time variations of the size and strength of flow vortices due to free convection heat transfer for the single-baffle case.

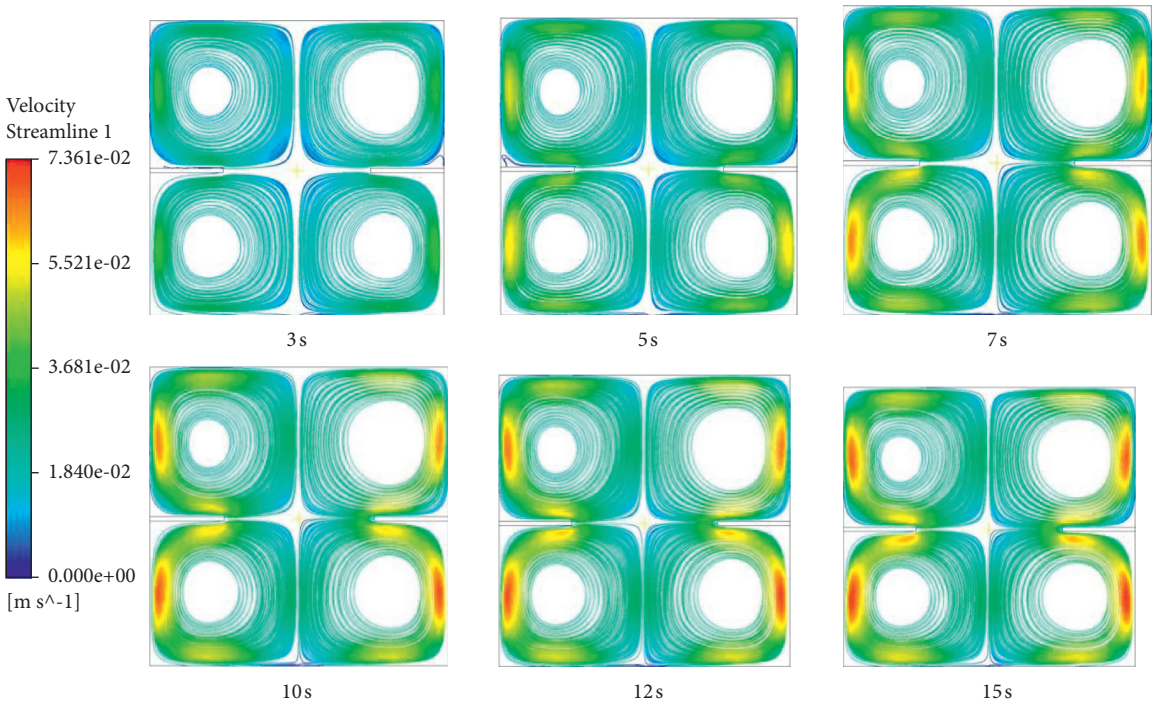

Figure 10: Time variations of the size and strength of flow vortices due to free convection heat transfer for the symmetric double-baffle case.

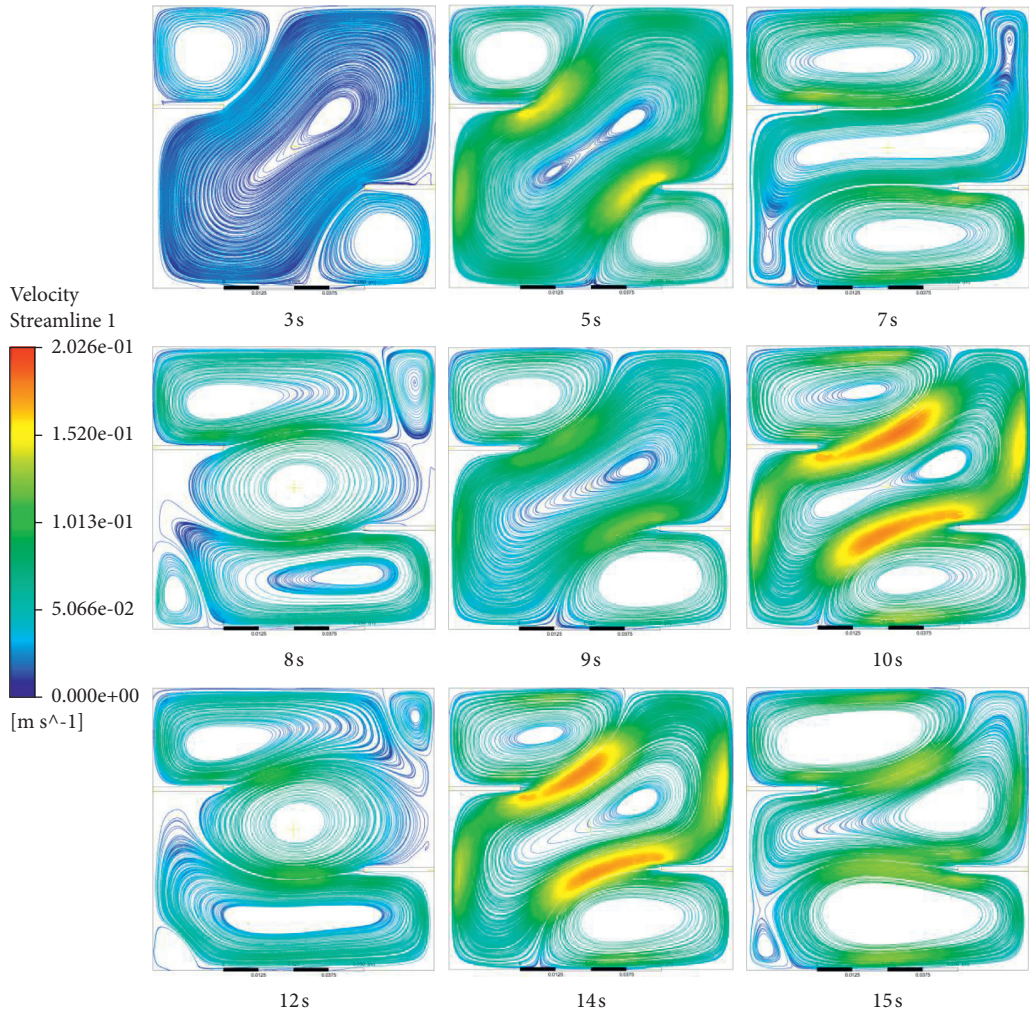

Figure 11: Time variations of the size and strength of flow vortices due to free convection heat transfer for the asymmetric double-baffle case.

In the symmetric case, due to the minor change in the size and features of vortices, the von Mises stress subsequently approaches the constant value of 0.8 Pa. It can be concluded that the baffle(s) and fluid reached a state of balance causing no variations in the baffle(s) loading over time.

In the asymmetric double-baffle case, large-amplitude fluctuations in the von Mises stress were observed after 3 s. Although the range of fluctuations was below 2 Pa, these fluctuations, due to feature and size variations of the flow vortices, never meet the stabilized situation, between the baffle(s) and fluid, leading to the persisting fluctuations of the von Mises stress in the baffle(s).

Figure 13 presents flow velocity variations at the center of the enclosure versus time for the three cases. In the single-baffle case, the velocity magnitude became almost constant after about 6 s. In the symmetric double-baffle case, it also reaches the constant value of 0.0007. Symmetric vortices developed at the top and bottom of the enclosure in this case practically led to quite an insignificant flow velocity at the center of the enclosure (Figure 8). In the asymmetric case, the flow velocity has gradually increased while it is fluctuating. As mentioned above, the reason lays size and features variations of vortices.

Table 5 presents the average Nusselt number over the hot wall and the von Mises stress. The comparison of the three cases shows that the highest Nusselt number occurred for the case with one elastic baffle. The single-baffle case also had the largest von Mises stress, which is due to this case having larger vortices among the three cases.

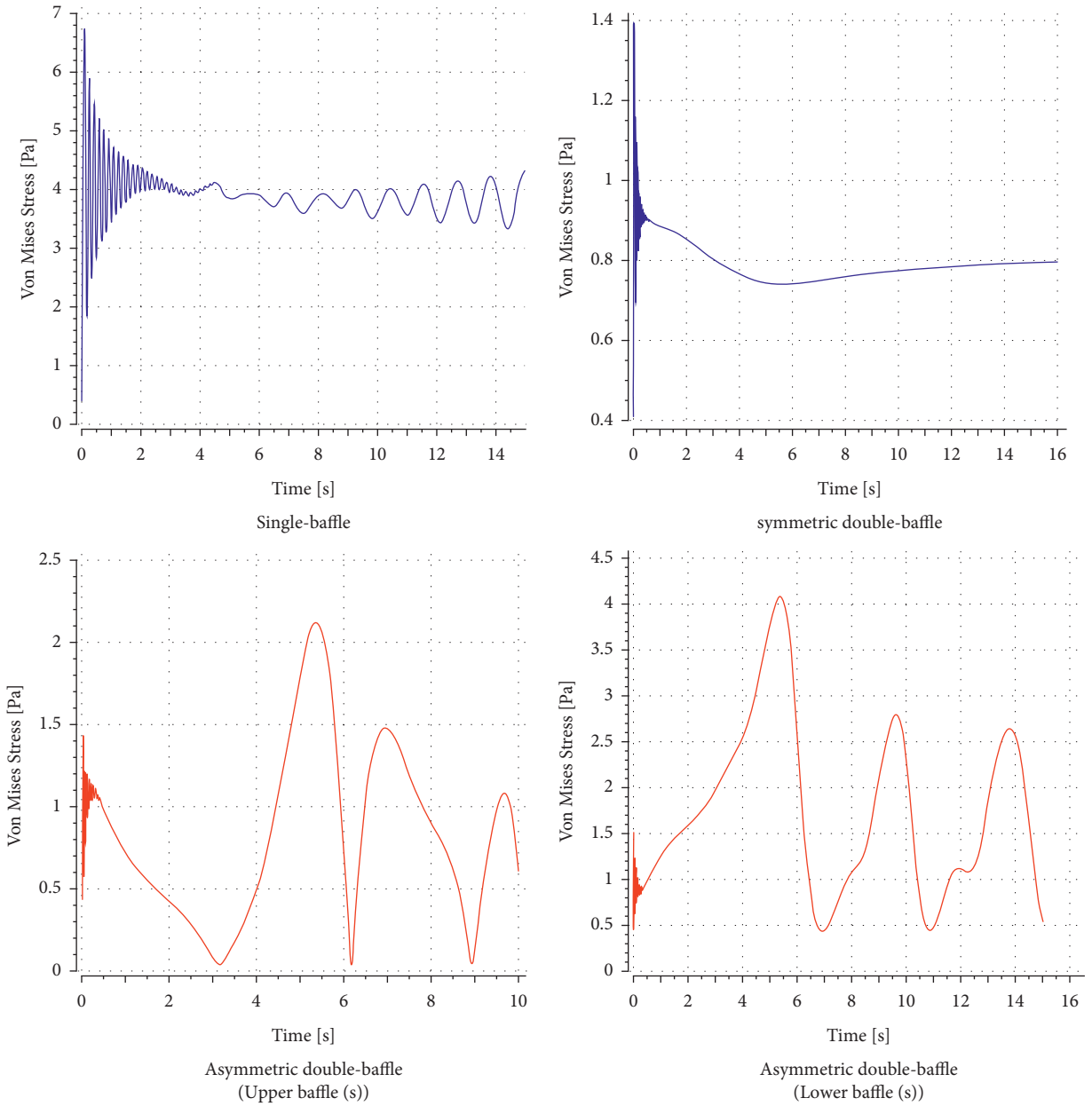

Figure 12: Variation of von Mises stress in the baffles over time.

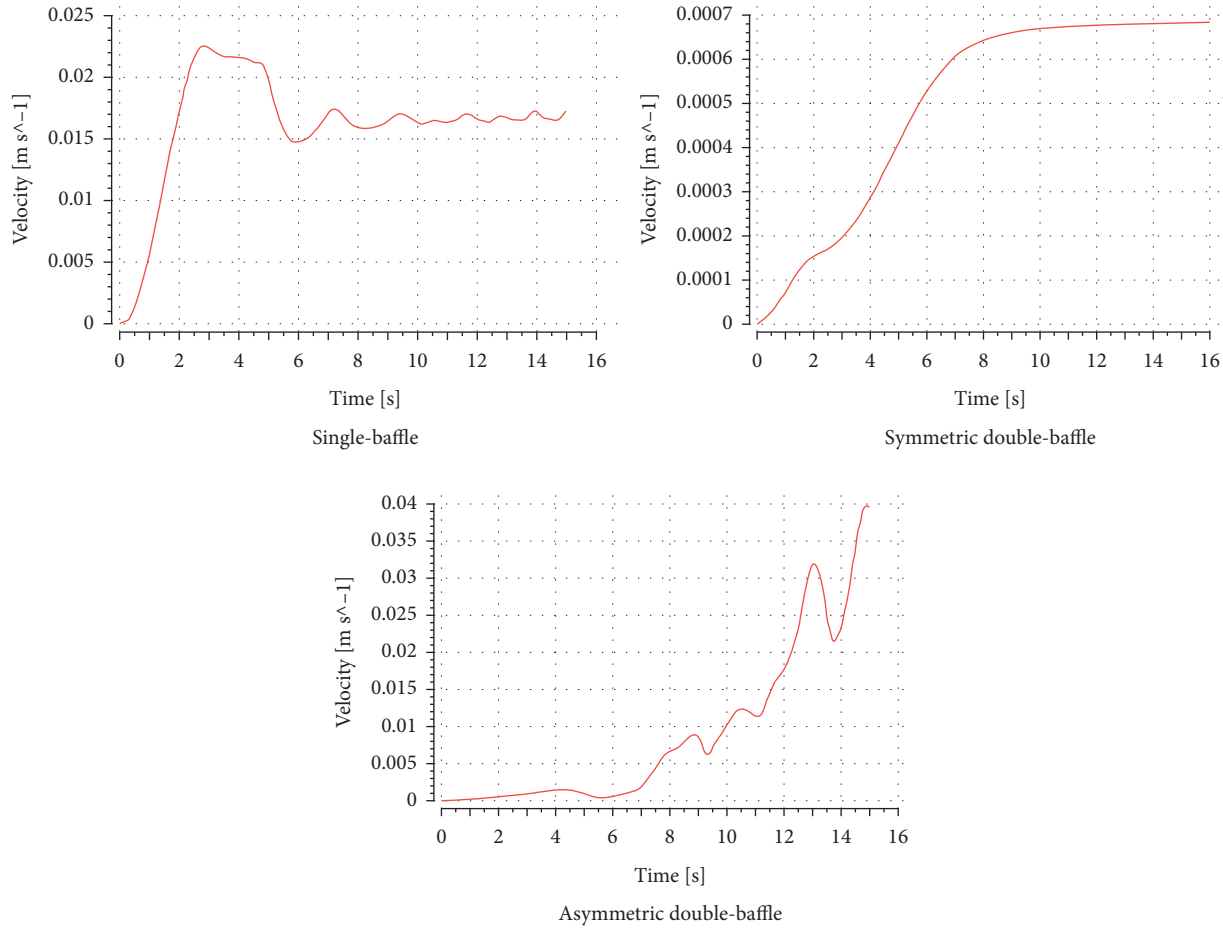

Figure 13: Variations of local speed at the center of the enclosure for single-baffle, asymmetric double-baffle, and symmetric double-baffle cases.

Table 5: Numerical values of the average Nusselt number over the hot wall and the von Mises stress at the baffle(s) rood in the steady state.

d/A	Solid	Single-baffle	Symmetric double-baffle	Asymmetric double-baffle	
Nu	16.5	19.17	16.5	13.1	
von Mises stress (Pa)	—	4.0	0.8	Upper <1	Lower <2

6. Conclusion

Fluid-solid interactions have sparked a heated debate recently. Although investigated by many researchers, the interaction between buoyancy-driven flow and mounted baffles on the side wall of an enclosure has not been studied thoroughly. Moreover, there are a few studies that considered the transient and unsteady convective heat transfer and fluctuations of baffle due to the flow forces imposed on that. Because of the temperature differences and physical properties of the fluid and the enclosure dimensions, which trigger a turbulent feature ($Ra > 10^7$), the fluid flow was simulated by the k-ε model. The baffles were assumed to be a kind of rubber assured that the fluctuations happened in the elastic range. A two-way algorithm along with the finite element method was employed in ANSYS Workbench software to simultaneously solve the equations governing the fluid flow and the solid phase. The dynamic mesh method was employed to account for the change in the location of the fluid domain at a new time step. The results represent various configurations of baffles and governing variables such as Nusselt number, von Mises stress, vortices' size and feature, and the flow velocity. The main conclusions are summarized as follows:

(i) It was found that the elastic baffle increases the heat transfer rate in comparison to the rigid baffle.

(ii) Nusselt number variations reached a relatively constant value after 2 s for all cases. However, it meets minor fluctuations over time in the asymmetric case.

(iii) The single-baffle case shows the highest average Nusselt number. Also, the symmetric double-baffle case had a higher Nusselt number than the asymmetric case.

(iv) In the single-baffle case, the baffle experiences fatigue loading, and there is an increase in the stress variations amplitude after 6 s.

(v) A high-amplitude fluctuation occurred in the von Mises stress in the asymmetric double-baffle case, the fluctuations were substantial until about 0.5 s.

(vi) In the asymmetric double-baffle case, no fluctuating variations were observed in the value of stress during the time. In the symmetric case, the velocity is very low, and it does not experience any fluctuations.

7. Future Directions

The effects of Ra numbers on the von Mises, heat transfer, fluid flow, and baffle fluctuation should be investigated in the future. Moreover, the other configurations of cavity and baffles position could be assessed. The fluid and baffle properties and also the position of the hot side on the average Nu can be considered for the next studies.

Abbreviations

k:	Thermal conductivity
ε:	Turbulent kinetic energy dissipation rate
Ra:	Rayleigh number
T_C:	Cold source temperature
T_h:	Hot source temperature
L:	Baffle length
σ:	Stress tensor
d_S:	Solid displacement vector
F_v:	Resultant volumetric force
S:	Second Piola–Kirchhoff stress tensor
α_S and α_f:	Thermal diffusion of the solid and fluid, respectively
P:	Fluid pressure
ρ_S:	Solid density
ρ_f:	Fluid density
ϑ_f:	Kinematic viscosity
g_y:	Gravitational acceleration
β:	Coefficient of volumetric expansion
μ:	Dynamic viscosity
μ_t:	Effective turbulent viscosity
τ:	Shear stress
C_μ:	Viscosity constant
σ_k and σ_ε:	Effective turbulent Prandtl
$C_{1\varepsilon}$ and $C_{2\varepsilon}$:	Constants appearing in the transport equation for ε
Nu:	Nusselt number
Re:	Reynolds number.

Data Availability

The data used to support the findings of this study are included within the article.

Conflicts of Interest

The authors declare that they have no conflicts of interest.

References

[1] R. Y. Farsani, A. Mahmoudi, and M. Jahangiri, "How a conductive baffle improves melting characteristic and heat transfer in a rectangular cavity filled with gallium," *Thermal Science and Engineering Progress*, vol. 16, Article ID 100453, 2020.

[2] R. Y. Farsani, F. Raeiszadeh, M. Jahangiri, and M. Afrand, "Melting characteristics of paraffin wax in a rectangular cavity under steady rotations," *Journal of the Taiwan Institute of Chemical Engineers*, vol. 113, pp. 135–141, 2020.

[3] F. Selimefendigil, H. F. Oztop, and A. J. Chamkha, "MHD mixed convection in a nanofluid filled vertical lid-driven cavity having a flexible fin attached to its upper wall," *Journal of Thermal Analysis and Calorimetry*, vol. 135, no. 1, pp. 325–340, 2019.

[4] F. Selimefendigil and H. F. Öztop, "Forced convection in a branching channel with partly elastic walls and inner L-shaped conductive obstacle under the influence of magnetic field," *International Journal of Heat and Mass Transfer*, vol. 144, Article ID 118598, 2019.

[5] F. Selimefendigil and H. F. Öztop, "Effects of an inner stationary cylinder having an elastic rod-like extension on the mixed convection of CNT-water nanofluid in a three dimensional vented cavity," *International Journal of Heat and Mass Transfer*, vol. 137, pp. 650–668, 2019.

[6] F. Selimefendigil and H. F. Öztop, "MHD mixed convection of nanofluid in a flexible walled inclined lid-driven L-shaped cavity under the effect of internal heat generation," *Physica A: Statistical Mechanics and Its Applications*, vol. 534, Article ID 122144, 2019.

[7] I. Hashim, A. I. Alsabery, M. A. Sheremet, and A. J. Chamkha, "Numerical investigation of natural convection of Al2O3-water nanofluid in a wavy cavity with conductive inner block using Buongiorno's two-phase model," *Advanced Powder Technology*, vol. 30, no. 2, pp. 399–414, 2019.

[8] F. Selimefendigil and H. F. Öztop, "Fluid-solid interaction of elastic-step type corrugation effects on the mixed convection of nanofluid in a vented cavity with magnetic field," *International Journal of Mechanical Sciences*, vol. 152, pp. 185–197, 2019.

[9] A. I. Alsabery, F. Selimefendigil, I. Hashim, A. J. Chamkha, and M. Ghalambaz, "Fluid-structure interaction analysis of entropy generation and mixed convection inside a cavity with flexible right wall and heated rotating cylinder," *International Journal of Heat and Mass Transfer*, vol. 140, pp. 331–345, 2019.

[10] A. Keyhani Asl, S. Hossainpour, M. M. Rashidi, M. A. Sheremet, and Z. Yang, "Comprehensive investigation of solid and porous fins influence on natural convection in an inclined rectangular enclosure," *International Journal of Heat and Mass Transfer*, vol. 133, pp. 729–744, 2019.

[11] A. Bendaraa, M. M. Charafi, and A. Hasnaoui, "Numerical study of natural convection in a differentially heated square cavity filled with nanofluid in the presence of fins attached to walls in different locations," *Physics of Fluids*, vol. 31, no. 5, Article ID 052003, 2019.

[12] Y. Menni, A. Chamkha, C. Zidani, and B. Benyoucef, "Baffle orientation and geometry effects on turbulent heat transfer of a constant property incompressible fluid flow inside a

rectangular channel," *International Journal of Numerical Methods for Heat and Fluid Flow*, vol. 30, no. 6, pp. 3027–3052, 2019.

[13] F. Keramat, A. Azari, H. Rahideh, and M. Abbasi, "A CFD parametric analysis of natural convection in an H-shaped cavity with two-sided inclined porous fins," *Journal of the Taiwan Institute of Chemical Engineers*, vol. 114, pp. 142–152, 2020.

[14] Z. Li, A. K. Hussein, O. Younis, M. Afrand, and S. Feng, "Natural convection and entropy generation of a nanofluid around a circular baffle inside an inclined square cavity under thermal radiation and magnetic field effects," *International Communications in Heat and Mass Transfer*, vol. 116, Article ID 104650, 2020.

[15] P. Gokulavani, M. Muthtamilselvan, Q. M. Al-Mdallal, and D. H. Doh, "Effects of orientation of the centrally placed heated baffle in an alternative configured ventilation cavity," *The European Physical Journal Plus*, vol. 135, no. 1, p. 23, 2020.

[16] M. Ghalambaz, E. Jamesahar, M. A. Ismael, and A. J. Chamkha, "Fluid-structure interaction study of natural convection heat transfer over a flexible oscillating fin in a square cavity," *International Journal of Thermal Sciences*, vol. 111, pp. 256–273, 2017.

[17] A. I. Alsabery, M. A. Sheremet, M. Ghalambaz, A. J. Chamkha, and I. Hashim, "Fluid-structure interaction in natural convection heat transfer in an oblique cavity with a flexible oscillating fin and partial heating," *Applied Thermal Engineering*, vol. 145, pp. 80–97, 2018.

[18] A. Raisi and I. Arvin, "A numerical study of the effect of fluid-structure interaction on transient natural convection in an air-filled square cavity," *International Journal of Thermal Sciences*, vol. 128, pp. 1–14, 2018.

[19] A. K. Hussein, M. Ghodbane, Z. Said, and R. S. Ward, "The effect of the baffle length on the natural convection in an enclosure filled with different nanofluids," *Journal of Thermal Analysis and Calorimetry*, vol. 147, pp. 1–23, 2020.

[20] M. Ghalambaz, S. A. M. Mehryan, A. I. Alsabery, A. Hajjar, M. Izadi, and A. Chamkha, "Controlling the natural convection flow through a flexible baffle in an L-shaped enclosure," *Meccanica*, vol. 55, no. 8, pp. 1561–1584, 2020.

[21] H. Saleh, I. Hashim, E. Jamesahar, and M. Ghalambaz, "Effects of flexible fin on natural convection in enclosure partially-filled with porous medium☆," *Alexandria Engineering Journal*, vol. 59, no. 5, pp. 3515–3529, 2020.

[22] R. Jetli, S. Acharya, and E. Zimmerman, "Influence of baffle location on natural convection in a partially divided enclosure," *Numerical Heat Transfer*, vol. 10, no. 5, pp. 521–536, 1986.

[23] H. Ambarita, K. Kishinami, M. Daimaruya, T. Saitoh, H. Takahashi, and J. Suzuki, "Laminar natural convection heat transfer in an air filled square cavity with two insulated baffles attached to its horizontal walls," *Thermal science and engineering*, vol. 14, no. 3, pp. 35–46, 2006.

[24] M. Jahangiri, M. Saghafian, and M. R. Sadeghi, "Effect of six non-Newtonian viscosity models on hemodynamic parameters of pulsatile blood flow in stenosed artery," *Journal of Computational and Applied Research in Mechanical Engineering*, vol. 7, no. 2, pp. 199–207, 2018.

[25] J. Moradicheghamahi, M. Jahangiri, M. Mousaviraad, and M. R. Sadeghi, "Computational studies of comparative and cumulative effects of turbulence, fluid–structure interactions, and uniform magnetic fields on pulsatile non-Newtonian flow in a patient-specific carotid artery," *Journal of the Brazilian Society of Mechanical Sciences and Engineering*, vol. 42, no. 10, pp. 1–22, 2020.

[26] B. Sharifzadeh, R. Kalbasi, M. Jahangiri, D. Toghraie, and A. Karimipour, "Computer modeling of pulsatile blood flow in elastic artery using a software program for application in biomedical engineering," *Computer Methods and Programs in Biomedicine*, vol. 192, Article ID 105442, 2020.

[27] M. Jahangiri, A. Haghani, R. Ghaderi, and S. M. Hosseini Harat, "Effect of non-Newtonian models on blood flow in artery with different consecutive stenosis," *ADMT Journal*, vol. 11, no. 1, pp. 79–86, 2018.

[28] J. Moradicheghamahi, J. Sadeghiseraji, and M. Jahangiri, "Numerical solution of the Pulsatile, non-Newtonian and turbulent blood flow in a patient specific elastic carotid artery," *International Journal of Mechanical Sciences*, vol. 150, pp. 393–403, 2019.

[29] B. Sharifzadeh, R. Kalbasi, and M. Jahangiri, "The effect of turbulence model on predicting the development and progression of coronary artery atherosclerosis," *Journal of Computational and Applied Research in Mechanical Engineering*, vol. 10, no. 1, pp. 183–199, 2020.

[30] M. Yadegari, M. Jahangiri, and Y. Mehrdad, "Simulation of non-uniform magnetic field impact on non-Newtonian and pulsatile blood flow," *Journal of Advanced Research in Fluid Mechanics and Thermal Sciences*, vol. 57, no. 1, pp. 86–99, 2019.

[31] M. R. Sadeghi, M. Jahangiri, and M. Saghafian, "The impact of uniform magnetic field on the pulsatile non-Newtonian blood flow in an elastic stenosed artery," *Journal of the Brazilian Society of Mechanical Sciences and Engineering*, vol. 42, no. 11, pp. 1–15, 2020.

[32] M. Saghafian, M. Reisi, and M. Jahangiri, "Distribution numerical, raising smoke and contamination condense distribution stimulating in chimney exit," *International Journal of Innovation and Applied Studies*, vol. 6, no. 1, pp. 1–13, 2014.

[33] M. Jahangiri, M. Saghafian, and M. R. Sadeghi, "Effects of non-Newtonian behavior of blood on wall shear stress in an elastic vessel with simple and consecutive stenosis," *Biomedical and Pharmacology Journal*, vol. 8, no. 1, pp. 123–131, 2015.

[34] M. Jahangiri, M. Saghafian, and M. R. Sadeghi, "Numerical simulation of non-Newtonian models effect on hemodynamic factors of pulsatile blood flow in elastic stenosed artery," *Journal of Mechanical Science and Technology*, vol. 31, no. 2, pp. 1003–1013, 2017.

[35] M. Jahangiri, R. Y. Farsani, and A. A. Shamsabadi, "Numerical investigation of the water/alumina nanofluid within a microchannel with baffles," *Journal of Mechanical Engineering and Technology*, vol. 10, no. 2, pp. 67–76, 2019.

[36] S. Motahar and M. Jahangiri, "Transient heat transfer analysis of a phase change material heat sink using experimental data and artificial neural network," *Applied Thermal Engineering*, vol. 167, Article ID 114817, 2020.

[37] M. Jahangiri, M. Saghafian, and M. R. Sadeghi, "Numerical study of hemodynamic parameters in pulsatile turbulent blood flow in flexible artery with stenosis," in *Proceedings of the 22st Annual International Conference on Mechanical Engineering-Isme 2014*, Shahid Chamran University, Ahvaz, Iran, April 2014.

[38] M. Jahangiri, M. Saghafian, and M. R. Sadeghi, "Numerical simulation of hemodynamic parameters of turbulent and pulsatile blood flow in flexible artery with single and double stenoses," *Journal of Mechanical Science and Technology*, vol. 29, no. 8, pp. 3549–3560, 2015.

[39] M. Jahangiri, M. Saghafian, and M. R. Sadeghi, "Numerical study of turbulent pulsatile blood flow through stenosed artery using fluid-solid interaction," *Computational and mathematical methods in medicine*, vol. 2015, Article ID 515613, 10 pages, 2015.

[40] L. C. Demartini, H. A. Vielmo, and S. V. Möller, "Numeric and experimental analysis of the turbulent flow through a channel with baffle plates," *Journal of the Brazilian Society of Mechanical Sciences and Engineering*, vol. 26, no. 2, pp. 153–159, 2004.

[41] S. R. Blair and Y. W. Kwon, "Modeling of fluid–structure interaction using lattice Boltzmann and finite element methods," *Journal of Pressure Vessel Technology*, vol. 137, no. 2, p. 9, Article ID 021302, 2015.

[42] D. Koblar, J. Škofic, and M. Boltežar, "Evaluation of the young's modulus of rubber-like materials bonded to rigid surfaces with respect to Poisson's ratio," *Strojniški vestnik-Journal of Mechanical Engineering*, vol. 60, no. 7-8, pp. 506–511, 2014.